Coherent Smith-Purcell radiation in the millimeter-wave region from a short-bunch beam of relativistic electrons

Yukio Shibata, Shigeru Hasebe, Kimihiro Ishi, Shuichi Ono, and Mikihiko Ikezawa
Research Institute for Scientific Measurements, Tohoku University, Katahira, Sendai 980-77, Japan

Toshiharu Nakazato, Masayuki Oyamada, and Shigekazu Urasawa
Laboratory of Nuclear Science, Tohoku University, Mikamine, Sendai 982, Japan

Toshiharu Takahashi, Tomochika Matsuyama, Katsuhei Kobayashi, and Yoshiaki Fujita
Research Reactor Institute, Kyoto University, Kumatori, Osaka 690-04, Japan
(Received 5 September 1997)

Coherent Smith-Purcell radiation, generated by the passage of short-bunched electrons of 150 and 40 MeV above a lamellar-type grating, has been observed in the millimeter-wave region. The intensity of the coherent radiation is proportional to the square of the beam current, and is enhanced by a factor of $\sim 10^8$ in comparison with theoretical intensity of ordinary Smith-Purcell radiation. The enhancement factor is of the same order of magnitude as the number of electrons in a bunch. The intensity decreases with the increase of the beam height, or the distance of the beam from the grating, and the dependence on the beam height is expressed approximately by the modified Bessel function of the zeroth order. Owing to a relativistic effect the radiation is emitted in a narrow direction along the plane normal to the grating. The intensity of the radiation varies in a periodic way when the groove depth of the grating was changed. The observed properties of radiation are explained well by a three-dimensional theory of Smith-Purcell radiation, in which the coherence effect due to bunched electrons is taken into account. [S1063-651X(98)02801-3]

PACS number(s): 41.60.−m, 42.72.Ai

I. INTRODUCTION

Smith-Purcell radiation (SPR) is emitted by an electron moving near a metallic grating. Since the first experiment by Smith and Purcell [1], many investigations [2–10] have been carried out using low-energy electron beams of a few hundred keV or less. Well verified is the dispersion relation of SPR,

$$n\lambda = g(1/\beta - \cos\theta), \tag{1}$$

where λ and n are the wavelength and the order of SPR, respectively, g is the grating period, β the ratio of the velocity of electrons to the light velocity in vacuum, and θ the emission angle measured from the trajectory of the electron.

Experimentally, however, properties of SPR have not been studied well except for the dispersion relation. Using an electron beam of a special configuration of grazing incidence where the beam hit the grating, Bachheimer [6] and Burdette and Hughes [7] studied properties of SPR such as spectral distribution, monochromaticity and dependence of the intensity on the beam current. However, in the case of the ordinary configuration of the experiment where the trajectory of the electron is parallel to the surface of grating, properties of the SPR have scarcely been clarified. For example, the dependence of intensity of SPR on beam height, which is defined as the distance between the trajectory of beam and a surface of the grating, has not been observed. This is mainly due to the difficulty in controlling the trajectory and the cross-sectional size of the electron beam with the precision of the wavelength of the radiation.

According to the theory of Toraldo di Francia [11], the intensity P of SPR depends exponentially on the beam height h,

$$P = P_0 \exp\left(-\frac{4\pi h}{\beta\gamma\lambda}\right), \tag{2}$$

where P_0 is a constant and $\gamma = (1-\beta)^{-1/2}$ is the Lorentz factor. Equation (2) shows that, in the case of a low-energy electron beam ($\beta \ll 1$ and $\gamma \sim 1$), we have to bring the trajectory of the beam close to surface of the grating to generate intense radiation, since the intensity P decreases sharply with increasing the beam height h by an amount of the wavelength λ. If we use a high-energy beam ($\beta \sim 1$ and $\gamma \gg 1$), however, the intensity P decreases slowly with the beam height h, and an experimental advantage is that the required precision in controlling the beam position is relaxed by the factor γ. This is related to the fact that the electric field perpendicular to the direction of motion is increased by the factor γ compared with static field [12]. A practical advantage of the use of high-energy electron beams with the large Lorentz factor will be that we can utilize a high current beam of large cross section to generate intense SPR. In spite of the advantages, however, only a few studies were carried out by the use of relativistic electrons.

Recently, Doucas *et al.* [13] studied SPR in the far-infrared region using electrons of energy of 3.6 MeV ($\gamma = 7.1$) from a Van de Graaff accelerator. Woods *et al.* [14] have observed intense forward SPR of higher orders using a short-bunched electron beam of 2.8 MeV ($\gamma = 5.5$). Haeberle *et al.* [15] theoretically calculated the intensity of SPR for a wide range of the energy of the electron from 1 to 100 MeV.

Using a short-bunched beam of 42 MeV ($\gamma=82$) from a linear accelerator, we observed coherent SPR in the millimeter-wave region and reported in a qualitative way that the SPR intensity was enhanced by several orders of magnitude compared with the ordinary SPR [16]. We also observed that the intensity decreases almost proportionally to the square of the modified Bessel function of the order zero with the beam height h. A theoretical explanation of this result, however, has not been given.

Coherent SPR is emitted when the electrons are bunched. Radiation from every electron in a bunch adds coherently in the spectral region where the wavelength is comparable to or longer than the longitudinal length of the bunch [16]. Analogy of the coherent synchrotron radiation [17–19] and coherent transition radiation [20–22] suggests that the intensity of coherent SPR will be proportional to the square of beam current and is enhanced by a factor N_e compared with ordinary (incoherent) SPR, where N_e is the number of electrons in a bunch. The coherence effect in SPR from the bunched electrons, however, has not been fully formulated in the literature.

The purpose of the present experiment is twofold: one purpose is to study the coherence effect in SPR in a quantitative way. For this purpose, we formulate in this paper the theory of SPR including the coherence effect and analyze our experimental data using it. The other purpose is to investigate properties of SPR by the observation of coherently enhanced radiation in the millimeter-wave region. In the long-wave region, the parameters of the experiment such as the dimensions of the grating can be precisely determined and the analysis with the formulated theory is possible. Concerning the radiation intensity, we have observed and analyzed the dependence on the beam height, the radiation angle, and the depth of the grating grooves. Besides the two purposes, our special interest is in the relativistic effects in the radiation process due to the high energy of the electron.

We have generated SPR from a short-bunched beam of electrons, which passed by a metallic grating of the lamellar type. We have used two kinds of electron beams whose energies were different; a beam with an energy of 150 MeV from a linear accelerator at the Laboratory of Nuclear Science, Tohoku University (LNSTU) and a beam of 40 MeV from a linear accelerator at the Research Reactor Institute, Kyoto University (RRIKU).

In Sec. II of this paper, we develop a three-dimensional theory of SPR for the lamellar-type grating and formulate the coherence effect. The experimental system is described in Sec. III. In Sec. IV, experimental results and discussions are presented on the general properties of SPR, coherence effect due to the bunched electrons, the relativistic effects of dependence of the intensity on the beam height and on the emission angle, and the radiation intensity in relation to the shape of the grating. A part of the present results was briefly reported previously [23].

II. THEORY OF SMITH-PURCELL RADIATION

A. Smith-Purcell radiation from lamellar-type grating

Theoretical studies of SPR have been made by several investigators for various types of grating, using various approaches [24]. The general theory of SPR has been formulated by van den Berg [25]. For a particular shape of the lamellar-type grating, the generation of SPR has been treated by van der Berg and Tan as a two-dimensional problem using the modal expansion method [26]. They studied a case where electrons move perpendicularly to the groove of a grating and the moving electrons are uniformly distributed along the direction parallel to the grooves; the radiation is observed in a plane perpendicular to the ruling direction. In such a case, the intensity of the radiation is uniform along the ruling direction and is calculated as a two-dimensional problem in the plane of the observation. The two-dimensional treatment, however, is unsuitable to analyze our experiment, where the electrons move along a single line of a linear trajectory perpendicular to the groove.

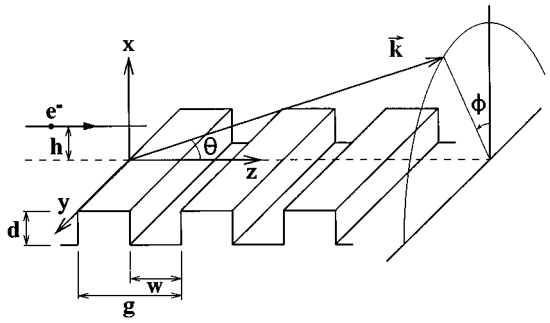

FIG. 1. Schematic layout of the geometry of the experiment. The electron moves with a speed v at a distance h parallel to a grating and perpendicular to the rulings.

Haebelre *et al.* [15] reviewed the theoretical studies and concluded that for a lamellar grating the modal expansion method is a simpler and more time saving way to calculate SPR than other approaches. Here we adopt the method to solve a three-dimensional problem to analyze our experimental results.

The lamellar grating is assumed to have ideal conductivity. We take a Cartesian coordinate system: an electron moves to the z direction with a constant velocity $v=\beta c$ along the trajectory $x=h$, $y=0$ as shown in Fig. 1. The grating are ruled parallel to the y axis and its ruled area is assumed to be large enough to ignore any boundary effect. We denote the grating period, width, and depth of the groove as g, w, and d, respectively. All quantities are expressed in SI units.

We consider the following Fourier components $\mathbf{E}_\omega$ and $\mathbf{H}_\omega$ of electric and magnetic fields:

$$\mathbf{E}(x,y,z,t)=\int\int \mathbf{E}_\omega(x,z,\eta,\omega)\exp[i(\eta y-\omega t)]d\eta d\omega, \tag{3}$$

$$\mathbf{H}(x,y,z,t)=\int\int \mathbf{H}_\omega(x,z,\eta,\omega)\exp[i(\eta y-\omega t)]d\eta d\omega. \tag{4}$$

The electric current has only the z component,

$$J_\omega(x,z,\eta,\omega)=\left(\frac{q}{2\pi}\right)^2 \exp(i\alpha_0 z)\,\delta(x-h), \tag{5}$$

where q is the charge of the electron, and $\alpha_0=\omega/v$.

Maxwell's equation reduces to the two-dimensional Helmholtz equations of $E_{\omega y}$ and $H_{\omega y}$,

$$\frac{\partial^2 E_{\omega y}}{\partial^2 x}+\frac{\partial^2 E_{\omega y}}{\partial^2 z}+(k^2-\eta^2)E_{\omega y}=i\,\frac{q}{4\pi^2}\left(\frac{\mu_0}{\varepsilon_0}\right)^{1/2}\frac{\eta}{\beta}\times\delta(x-h)\exp(\imath\alpha_0 z), \tag{6}$$

$$\frac{\partial^2 H_{\omega y}}{\partial^2 x}+\frac{\partial^2 H_{\omega y}}{\partial^2 z}+(k^2-\eta^2)H_{\omega y}=\frac{q}{4\pi^2}\frac{d}{dx}\,\delta(x-h)\times\exp(i\alpha_0 z), \tag{7}$$

where k is the absolute value of the wave vector, ω/c. The x and z components of $\mathbf{E}_\omega$ and $\mathbf{H}_\omega$ in Eqs. (3) and (4) are expressed in terms of $E_{\omega y}$ and $H_{\omega y}$. The solution of the Helmholtz equation in half space above the grating ($x\geqslant 0$) is written as

$$E^+_{\omega y}=E^c_{\omega y}+E^r_{\omega y}, \tag{8}$$

$$H^+_{\omega y}=H^c_{\omega y}+H^r_{\omega y}, \tag{9}$$

where $E^r_{\omega y}$ and $H^r_{\omega y}$ are the homogeneous solutions and $E^c_{\omega y}$ and $H^c_{\omega y}$ are the inhomogeneous ones. The solution $E^r_{\omega y}$ stands for the E-polarized component whose electric vector is parallel to the ruling of the grating, and the H-polarized component $H^r_{\omega y}$ has the electric vector parallel to the plane defined by the grating normal and the trajectory of the beam. The inhomogeneous solution corresponds to the charge field of the electron,

$$E^c_{\omega y}=\frac{q}{8\pi^2}\left(\frac{\mu_0}{\varepsilon_0}\right)^{1/2}\frac{\eta\alpha_0}{\beta\gamma_0}\exp[i(\alpha_0 z+\gamma_0|x-h|)], \tag{10}$$

$$H^c_{\omega y}=\frac{q}{8\pi^2}\,\mathrm{sgn}(x-h)\exp[i(\alpha_0 z+\gamma_0|x-h|)], \tag{11}$$

in which

$$\gamma_0=i(\alpha_0^2+\eta^2-k^2)^{1/2}. \tag{12}$$

Since α_0 is always larger than k, γ_0 is pure imaginary and Eqs. (10) and (11) express evanescent waves that move along z axis with the velocity of the electron and decrease exponentially away from the trajectory.

The homogeneous solutions are expanded in infinite series,

$$E^r_{\omega y}=\sum_{n=-\infty}^{\infty}E_n\exp[i(\alpha_n z+\gamma_n x)], \tag{13}$$

$$H^r_{\omega y}=\sum_{n=-\infty}^{\infty}H_n\exp[i(\alpha_n z+\gamma_n x)], \tag{14}$$

in which

$$\alpha_n=\alpha_0+\frac{2n\pi}{g}, \tag{15}$$

$$\gamma_n=(k^2-\alpha_n^2-\eta^2)^{1/2}. \tag{16}$$

When γ_n is real, the solution corresponds to SPR with the order n. The emission angles (θ,ϕ) of the SPR is related to α_n, η, and γ_n as

$$\gamma_n=k\,\sin\,\theta\,\cos\,\phi,$$

$$\eta=k\,\sin\,\theta\,\sin\,\phi,$$

$$\alpha_n=k\,\cos\,\theta. \tag{17}$$

The solution of the Helmholtz equation in the grooves ($x\leqslant 0$) is expressed as series of the cavity modes in the groove,

$$E^-_{\omega y}=\exp(i\alpha_0 Jg)\sum_{m=1}^{\infty}G_m\,\sin\left(\frac{m\pi z'}{w}\right)[\exp(-i\kappa_m x)-\Gamma_m\exp(i\kappa_m x)], \tag{18}$$

$$H^-_{\omega y}=\exp(i\alpha_0 Jg)\sum_{m=0}^{\infty}F_m\,\cos\left(\frac{m\pi z'}{w}\right)[\exp(-i\kappa_m x)+\Gamma_m\exp(i\kappa_m x)], \tag{19}$$

where z' is an local coordinate parallel to the z direction within a groove; $z=Jg+z'$ $(J=0,\pm1,\pm2,...)$, $\kappa_m=[k^2-\eta^2-(m\pi/w)^2]^{1/2}$, and $\Gamma_m=\exp(i2\kappa_m d)$.

Using boundary conditions on the grating and continuity conditions between the solutions of the upper half space and those in the grooves, we get a set of algebraic equations for the unknowns E'_n and H'_n,

$$\sum_{n=-\infty}^{\infty}\left(g\,\delta_{nl}+w\,\gamma_n\sum_{m=0}^{\infty}B_m\Phi^*_{mn}\Phi_{ml}\right)E'_n=-g\,\delta_{l0}+w\,\gamma_0\sum_{m=0}^{\infty}B_m\Phi^*_{m0}\Phi_{ml}, \tag{20}$$

$$\sum_{n=-\infty}^{\infty}\left(\gamma_n g\,\delta_{nl}-w\sum_{m=0}^{\infty}D_m\Psi^*_{mn}\Psi_{ml}\right)H'_n=g\,\gamma_0\,\delta_{l0}+w\sum_{m=0}^{\infty}D_m\Psi^*_{m0}\Psi_{ml},$$

$$l=0,\pm1,\pm2,..., \tag{21}$$

where E'_n and H'_n are related to the coefficients E_n and H_n of the homogeneous solution of Eqs. (13) and (14),

$$E_n=\frac{q}{8\pi^2}\left(\frac{\mu_0}{\varepsilon_0}\right)^{1/2}\frac{\eta}{\beta\gamma_0}\exp(i\gamma_0 h)E'_n, \tag{22}$$

$$H_n=\frac{q}{8\pi^2}\exp(i\gamma_0 h)H'_n. \tag{23}$$

In Eqs. (20) and (21), B_m, D_m, Φ_{mn}, and Ψ_{mn} are defined as follows:

$$B_m=\frac{2(1-\Gamma_m)}{\kappa_m(1+\Gamma_m)}, \tag{24}$$

$$D_m=\frac{2\kappa_m(\Gamma_m-1)}{(1+\delta_{m0})(\Gamma_m+1)}, \tag{25}$$

$$\Phi_{mn}=\frac{1}{w}\int_0^w \sin\left(\frac{m\pi z}{w}\right)\exp(-\imath\alpha_n z)dz, \tag{26}$$

$$\Psi_{mn}=\frac{1}{w}\int_0^w \cos\left(\frac{m\pi z}{w}\right)\exp(-\imath\alpha_n z)dz, \tag{27}$$

and Φ^*_{mn} and Ψ^*_{mn} are the conjugate complex of Φ_{mn} and Ψ_{mn}, respectively [27].

When the cross-sectional dimensions of the lamellar grating are known, we can solve Eqs. (20) and (21) to obtain the radiation field of SPR for any ω and η, i.e., wavelength λ or the emission angle θ and the azimuth angle ϕ.

In the case of $\eta=0$, i.e., when SPR is observed in the plane defined by the trajectory of the electron and the normal to the grating, Eq. (21) reduces to the equation of SPR in the xz plane, which has been studied by van den Bergh and Tan [26]. In this case, since $E_n=0$ from Eq. (22), SPR is completely polarized and the electric vector is in the observational plane.

It is pointed out here that the coefficients of Eqs. (20) and (21) show that there is a similarity relation in SPR with respect to the wavelength and the grating parameters. In other words, the angular distribution and the dependence of intensity on the groove depth, for example, generated with one grating is similar to those with another grating if the ratio of $\lambda:g:w:d$ is the same for the two gratings.

The intensity of SPR per unit period of grating is calculated from Poynting vector passing through a stripe infinitely long in the y direction with the width of the grating period in the z direction, placed far from the surface of the grating,

$$P_{\text{tot}}=\int_0^g\int_{-\infty}^{\infty}\int_{-\infty}^{\infty}\mathbf{N}_x dt\ dy\ dz \tag{28}$$

$$=2\int dz\ \text{Re}\left\{\int\int\ \frac{\omega}{k^2-\eta^2}\left(\varepsilon_0 H^{r*}_{\omega y}\frac{\partial E^r_{\omega y}}{\partial x}+\mu_0 H^{r*}_{\omega y}\frac{\partial H^r_{\omega y}}{\partial x}\right)d\eta d\omega\right\}, \tag{29}$$

where $\mathbf{N}_x$ stands for the x component of the Poynting vector. Using Eqs. (13) and (14) and periodic condition of the field, we obtain

$$P_{\text{tot}}=\sum_{\text{rad}} P_n=\sum_{\text{rad}} 2g\mu_0\int\int\ \frac{\omega\gamma_n}{k^2-\eta^2}\left(\frac{\varepsilon_0}{\mu_0}|E_n|^2+|H_n|^2\right)d\eta d\omega, \tag{30}$$

where the summation is taken over the radiation field having real γ_n and P_n stands for the intensity of the order n. Using the relations (17), (22), and (23), we get the monochromatic intensity of SPR of the order n per electron per unit wavelength per unit period of the grating,

$$\frac{dP_n}{d\lambda}=\frac{q^2n^2}{8\pi^2 g\lambda\varepsilon_0}\int\ \frac{\beta^2\sin^2\theta_n\cos^2\phi}{(1-\beta\cos\theta_n)^2(1-\sin^2\theta_n\sin^2\phi)}[Q(\theta_n)^2|E'_n|^2+|H'_n|^2]$$
$$\times\exp\left(-\frac{4\pi h}{\beta\gamma\lambda}\sqrt{1+(\beta\gamma\sin\theta_n\sin\phi)^2}\right)d\phi, \tag{31}$$

$$Q(\theta_n)^2=\left(\frac{\eta}{\beta|\gamma_0|}\right)^2=\frac{(\gamma\sin\theta_n\sin\phi)^2}{1+(\beta\gamma\sin\theta_n\sin\phi)^2}. \tag{32}$$

In Eq. (31), the wavelength and the emission angle θ_n are related by the dispersion relation of Eq. (1).

A real grating has a finite number of the grooves N_g, and the SPR intensity is N_g times Eq. (31), if N_g is large enough. When N_g is not so large, the intensity of the SPR of the order n emitted from the grating of N_g period is expressed as, in the unit of photon numbers per electron per relative bandwidth $d\lambda/\lambda=d\ln\lambda$,

$$\frac{dP^{\text{ph}}_n}{d\ln\lambda}=\frac{\alpha n^2}{4\pi^2}\int G_n(T)\frac{\beta^2\sin^2\theta\cos^2\phi}{(1-\beta\cos\theta)^2(1-\sin^2\theta\sin^2\phi)}[Q(\theta)^2|E'_n|^2+|H'_n|^2]\exp\left(-\frac{4\pi h}{\beta\gamma\lambda}\sqrt{1+(\beta\gamma\sin\theta\sin\phi)^2}\right)d\Omega, \tag{33}$$

where α is the fine-structure constant, and $d\Omega$ is solid angle, $d\Omega = \sin\theta\, d\theta\, d\phi$.

Since the phase difference of radiation emitted from subsequent grooves during the passage of the electron is $kg(1/\beta - \cos\theta)$, the factor $G_n(T)$ in Eq. (33) stands for the effect of superposition of radiation from each period of the grating:

$$G_n(T) = \left\{ \frac{\sin(N_g T)}{\sin T} \right\}^2, \tag{34}$$

$$T = \frac{g\pi}{\lambda} \left(\frac{1}{\beta} - \cos\theta \right). \tag{35}$$

The factor $G_n(T)$ has peaks at $T = m\pi$, $m = 1,2,...,M$ where M is the maximum integer bounded by $2g/\lambda$. When the number N_g of the period of the grating increases, the factor $G_n(T)$ approaches the delta function $(gN_g/\lambda)[\delta(\theta - \theta_n)/\sin\theta_n]$. We get the monochromatic intensity of SPR in photon number by the integration of Eq. (33) with respect to the solid angle, which gives the factor $N_g \hbar\omega$ to Eq. (31).

When the number of grooves is large, the factor $G_n(T)$ varies as a function of θ more rapidly than other factors in Eq. (33). The bandwidth $\Delta\lambda$ of SPR at wavelength λ is determined by the factor $G_n(T)$ and is expressed by

$$\frac{\lambda}{\Delta\lambda} = |n| N_g. \tag{36}$$

In numerical computation, we have truncated the various series in Eqs. (20) and (21) and have reduced the infinite system of Eqs. (20) and (21) to a finite system [26]. The computation was carried out by increasing the number of terms taken into account in the summation in Eqs. (20) and (21), and consequently by increasing the size of the dimension of the matrix of the finite equation system. The procedure was stopped as soon as the relative change of the values $|H'_{-1}|^2$ and $|E'_{-1}|^2$ turned out to be less than 1%. In some cases, however, the solution $|E'_{-1}|^2$ of the finite system had not converged and showed numerical oscillation with the increase of the size of the matrix. In such cases, we estimated the value around which the solution oscillated and adopted it as the solution; the numerical accuracy of the solution was estimated to be better than 10%.

B. Coherent SPR from bunched electrons

When the electrons are bunched, superposition of radiation from each electron in a bunch is observed. We formulate the coherence effect due to the bunched electrons, assuming that the number of electrons in the bunch is large and that the observational point of SPR is far from the grating.

As shown in Sec. II A, the Coulomb field of the electron is expanded by the evanescent waves, which moves along the z axis with the velocity of the electron. The evanescent waves are diffracted by the grating, and waves that have real γ_n are propagating into free space as SPR. Therefore, the phase difference $\Delta\psi$ between SPR emitted from an electron with the position $\mathbf{X}(X,Y,Z)$ and that from the electron at the bunch center (0,0,0), which is taken as the origin of the position vector of the electrons, is considered to be equal to the phase difference of the evanescent waves of the electrons,

$$\Delta\psi = \alpha_0 Z + \eta Y + \gamma_0 X. \tag{37}$$

The radiation field is calculated by superposition of SPR from the whole electrons in the bunch,

$$E_{b\omega} = \sum_{j=1}^{N_e} E_{0\omega} \exp[i(\alpha_0 Z_j + \eta Y_j + \gamma_0 X_j)], \tag{38}$$

where $E_{0\omega}$ is the radiation field of SPR from the electron at the bunch center. Since any order of SPR is expressed by Eq. (38), the intensity of SPR of the order n from the bunch is

$$\frac{dP_{n,\mathrm{bunch}}}{d\lambda} = N_e[1 + N_e f(\lambda)] \frac{dP_n}{d\lambda}, \tag{39}$$

where $dP_n/d\lambda$ is the SPR intensity from an electron of Eq. (31). The bunch form factor $f(\lambda)$ is defined, using the density distribution function $S(X,Y,Z)$ of electrons in the bunch, as

$$f(\lambda) = \left| \int\int\int S(X,Y,Z) \exp(-|\gamma_0| X) \times \exp\left[ik \left(Y \sin\theta_n \cos\phi + \frac{Z}{\beta} \right) \right] dX\, dY\, dZ \right|^2, \tag{40}$$

where k is wave number, $2\pi/\lambda$.

The bunch form factor is expressed as the product of a longitudinal form factor and a transverse one, $f(\lambda) = f_L(\lambda) f_T(\lambda)$, on the assumption that the longitudinal distribution function $S_L(Z)$ of electrons in the bunch has no correlation with the transverse one $S_T(X,Y)$:

$$f_T(\lambda) = \left| \int S_T(X,Y) \exp(-|\gamma_0| X) \times \exp\left(i2\pi \frac{Y \sin\theta_n \sin\phi}{\lambda} \right) dX\, dY \right|^2, \tag{41}$$

$$f_L(\lambda) = \left| \int S_L(Z) \exp\left(i2\pi \frac{Z}{\lambda} \right) dz \right|^2, \tag{42}$$

where

$$|\gamma_0| = \frac{2\pi}{\beta\gamma\lambda} \sqrt{1 + (\beta\gamma \sin\theta_n \sin\phi)^2}. \tag{43}$$

In Eq. (42) we have assumed that the energy of the beam is high and $\beta \sim 1$.

The value of the form factor $f(\lambda)$ depends on the dimension of the bunch, σ, as well as on the wavelength of radiation. In the short-wavelength region, or $\lambda \ll \sigma$, the value of the form factor is negligibly small and we observe only incoherent radiation $dP_{n,\mathrm{incoh}}/d\lambda$:

$$\frac{dP_{n,\mathrm{bunch}}}{d\lambda} = N_e \frac{dP_n}{d\lambda} = \frac{dP_{n,\mathrm{incoh}}}{d\lambda} \qquad \text{for} \qquad \lambda \ll \sigma. \tag{44}$$

In the long-wavelength region, or $\lambda > \sigma$, the $f(\lambda)$ becomes much larger than $1/N_e$ and we observe coherent radiation:

$$\frac{dP_{n,\mathrm{bunch}}}{d\lambda} = N_e^2 f(\lambda)\,\frac{dP_n}{d\lambda} = N_e f(\lambda)\,\frac{dP_{n,\mathrm{incoh}}}{d\lambda} \quad \text{for} \quad \lambda > \sigma. \tag{45}$$

The coherent SPR intensity is proportional to the square of the beam current and is enhanced $N_e f(\lambda)$ times in comparison with the ordinary intensity without the coherence effect, $dP_{n,\mathrm{incoh}}/d\lambda$. When the wavelength is long enough, i.e., $\lambda \gg \sigma$, the form factor $f(\lambda)$ approaches asymptotically to unity.

The longitudinal form factor of Eq. (42) has the same form as the one in coherent synchrotron radiation [19] and transition radiation [22]. However, the transverse form factor of Eq. (41) is different from the transverse one of the other radiations. The form factor Eq. (41) shows that SPR emitted from the electrons that have a common Y coordinate is in phase and that its amplitude depends exponentially on the beam height h, $\exp[-|\gamma_0|(h+X)]$. Hence the distribution of electrons in the X direction causes no negative interference in coherent SPR, even if the cross section of the beam is large in comparison with the wavelength. This suggests that the intensity of coherent SPR does not decrease so rapidly with the variation of the emission angle θ, whereas the coherence effect in synchrotron radiation and in transition radiation sharply decreases with the emission angle θ [22,28].

For the Gaussian distribution of electrons in a bunch, we can calculate the bunch form factor as follows: for the longitudinal distribution function, $S_L(Z) = \exp[-(Z/\sigma_L)^2]/(\pi^{1/2}\sigma_L)$, we get

$$f_L(\lambda) = \exp\left[-2\left(\frac{\pi\sigma_L}{\lambda}\right)^2\right]. \tag{46}$$

For the transverse one $S_T(X,Y) = \exp[-(X^2+Y^2)/\sigma_T^2]/(\pi\sigma_T^2)$, we obtain

$$f_T(\lambda) = \frac{1}{\pi}\exp\left[2\left(\frac{\pi\sigma_T}{\beta\gamma\lambda}\right)^2\right]\left[\mathrm{erfc}\left(-\frac{h}{\sigma_T}+\frac{|\gamma_0|\sigma_T}{2}\right)\right]^2, \tag{47}$$

where $\mathrm{erfc}(x)$ is the error function.

Here, we estimate the value of the form factor for the present experiment at LNSTU. From the analysis of the spectrum of coherent diffraction radiation, the bunch shape of the 150-MeV beam used in the experiment is known to be nearly a Gaussian with the bunch length, or the full width at half maximum (FWHM), of 0.2 mm [29]. Therefore, in the millimeter-wave region the longitudinal bunch length is shorter than wavelengths. We get $f_L(\lambda) = 0.75$ at $\lambda = 1$ mm from Eq. (46). Using Eq. (47), we calculate the transverse bunch form factor, on the assumption of a Gaussian distribution of electrons in a circular cross section with the width (FWHM) of 2.5 mm. The result is $f_T(\lambda) \sim 1.0$ at the wavelengths $\lambda \geqslant 1$ mm. Hence $f(\lambda) > 0.75$ at $\lambda > 1$ mm and it is expected that we can observe coherent radiation in the millimeter wave region.

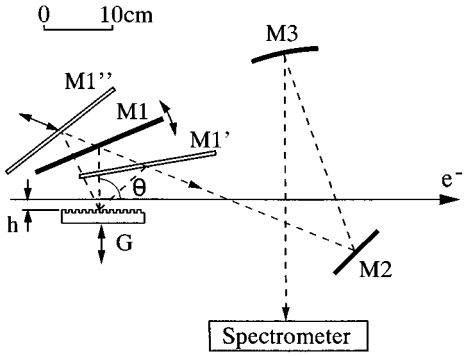

FIG. 2. Schematic diagram of experimental setup. G: grating; $M1$,$M2$: plane mirrors; $M3$: collecting mirror; θ : emission angle; h: beam height. The broken lines show the optical axes, and the mirror $M1$ is moved along positions $M1'$ and $M1''$.

III. EXPERIMENT

A schematic diagram of the experimental setup at LNSTU is shown in Fig. 2. The electrons of 150 MeV from the S-band linear accelerator passed near a grating G. The duration of a burst of electrons was 5 ns, and its repetition rate was 25 Hz. The energy spread of the electrons was 0.5%, and the average beam current was typically 10 nA. Hence the average number of electrons per bunch was 1.8×10^8.

The cross section of the beam was nearly circular, and the size of the beam (FWHM) was about 2.5 mm in diameter. The beam height h was usually set at 5 mm. When we examined the dependence of intensity on the beam height, the grating was moved along the direction perpendicular to the beam trajectory and the height h was varied from 2.5 to 45 mm.

The SPR was collected by a system of which the optical axis was in the plane including the trajectory of the beam and the normal to the grating. The SPR generated with the grating G in Fig. 2 was reflected by plane mirrors $M1$ and $M2$ and was collected by a spherical mirror $M3$. The mirror $M1$ was slid horizontally and was rotated simultaneously around a vertical axis so as to reflect the SPR toward $M2$ without the deviation of the optical axis. The radiation was led to a grating-type far-infrared spectrometer that covered the wavelength region from 0.1 to 6 mm. The radiation was detected with a helium-cooled Si bolometer.

If we assume that SPR was emitted from a line source on the grating surface, then the acceptance angle of the optical system was 50 mrad in the meridional plane defined by the grating normal and the trajectory of the electron and it was 88 mrad in the sagittal plane. Therefore, the SPR observed in the direction $(\theta, \phi = 0)$ included radiation emitted within the direction $\theta \pm 25$ mrad and $|\phi| \leqslant 44$ mrad.

The spectrometer was equipped with a polarizer, and in our experiment the H-polarized component and the V-polarized one in Sec. IV correspond to the H-polarized solution and the E-polarized one of Eqs. (22) and (23), respectively.

To determine the absolute intensity of the observed SPR, the measuring system was calibrated with a blackbody radiation source of 1200 K. Uncertainty of the absolute value was estimated to be a factor of 1.5 around $\lambda = 1$ mm.

We prepared five lamellar-type gratings ($G1-G5$) made

TABLE I. Lamellar-type gratings used in the experiment.

	Period g (mm)	Width of groove w (mm)	Depth of groove d (mm)	Number of grooves N_g
$G1$	2.0	1.0	1.0	60
$G2$	6.0	3.0	1.0	20
$G3$	6.0	3.0	3.0	20
$G4$	6.0	3.0	6.0	20
$G5$	8.0	4.0	1.0	15
$G6$	6.0	3.0	0.0–15.0	20
$G7$	12.0	6.0	0.0–15.0	15

of aluminum. The period, width, and depth of the groove are listed in Table I.

The experimental setup at RRIKU was similar to that of LNSTU, and the measuring system had the acceptance angle of 33 mrad in the meridional plane and of 72 mrad in the sagittal plane. The beam conditions were as follows. The energy was 40 MeV, a duration of macropulse was 33 ns, and its repetition was 55 pulse/s. The average beam current was 1.5 μA, and hence the number of electrons per bunch was 4×10^9.

The beam from the L-band linear accelerator of RRIKU was collimated to the size of 10×12 mm^2 in cross section by passing it through an aluminum block [16] except for the experiment to measure the dependence of the SPR intensity on the azimuth angle ϕ, in which the beam was collimated to the circular cross section of 12 mm in diameter. To observe the dependence of the intensity on the azimuth angle ϕ, we rotated the grating around the electron beam as shown in Fig. 3.

At RRIKU we prepared additional lamellar gratings of which depths of the grooves were variable from 0 to 15 mm. Their structure are schematically shown in Fig. 4 and the parameters of the gratings ($G6$,$G7$) are listed in Table I.

IV. EXPERIMENTAL RESULTS AND DISCUSSION

A. General properties of SPR

In this section two results are presented to verify that the observed radiation is SPR.

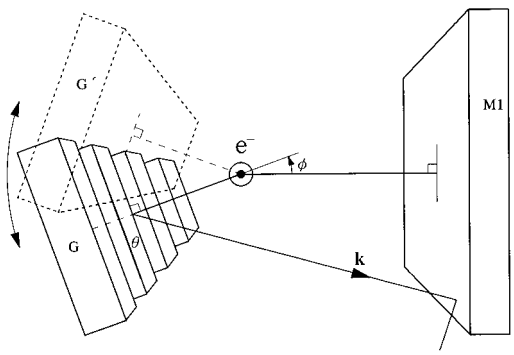

FIG. 3. Schematic diagram to observe the dependence of the SPR intensity on the azimuth angle ϕ. The grating G is rotated around the electron beam.

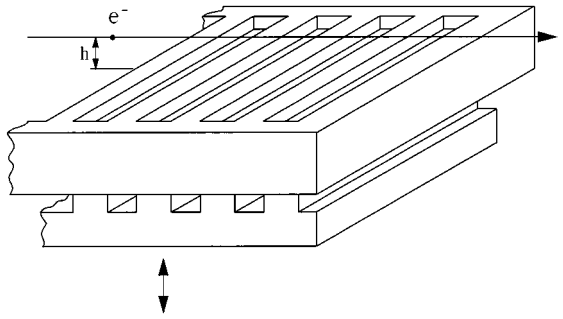

FIG. 4. The lamellar grating used to observe the dependence of the SPR intensity on the depth of the groove.

1. Dispersion relation

To observe the monochromatic emission of SPR, we scanned emission angle θ from 20 to 120 degrees by moving the mirror $M1$ in Fig. 2. The spectrometer was set at a fixed wavelength. Figure 5 shows one of the results by the 150-MeV electrons obtained with the gratings $G2$, $G3$, and $G4$. The angular distributions of SPR at the wavelengths of 1.3, 2.4, and 3.0 mm are shown by solid, dotted, and dashed curves, respectively. Every curve has one or a few peaks, except for the scan at $\lambda=3$ mm with the grating $G3$, in which SPR is not clearly observed. The figure shows that the intensity of SPR depends on the groove depth and the wavelength. This point is discussed further in Sec. IV D.

In Fig. 5, the most intense peak of each curve corresponds to the first order of SPR. The dispersion relation of the first order of SPR measured by the 150-MeV electron with the five gratings in Table I is shown in Fig. 6. Three curves in

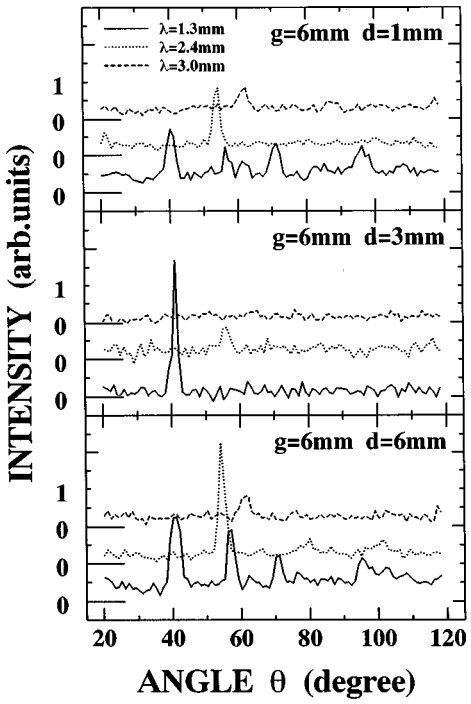

FIG. 5. Angular distribution of monochromatic SPR at $\lambda=1.3$, 2.4, and 3.0 mm observed with the three gratings $G2$, $G3$, and $G4$ in Table I. The energy of the electron is 150 MeV.

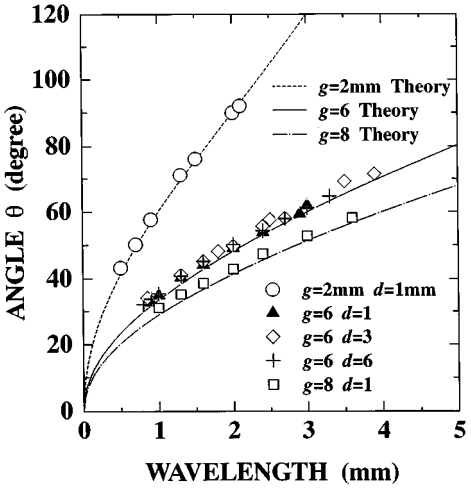

FIG. 6. Dispersion relation of SPR observed by the electron beam of 150 MeV. The three curves show the theoretical relation of Eq. (1) in the text.

the figure show the theoretical relation of Eq. (1). The experiment agrees well with theory. A similar result with the 40-MeV electron was reported previously [16].

2. Monochromaticity

Using the 40-MeV beam, we measured the spectrum of SPR with the grating-type spectrometer; an example is shown in Fig. 7. The mirror $M1$ in Fig. 2 was set at the direction θ so as to select the wavelength of 3 mm. The observed bandwidth (FWHM) in Fig. 7 was 0.17 mm. The resolution of the spectrometer was 0.09 mm at $\lambda = 3$ mm.

The finite number (N_g) of the grooves of the grating, which is 20 for the present case, results in monochromatic radiation with a finite bandwidth. This value was calculated as 0.15 mm from Eq. (36) with $N_g = 20$. The convolution of the width by the resolution of the spectrometer was evaluated as $\sqrt{0.09^2 + 0.15^2} = 0.17$ mm, which is in agreement with the observed width.

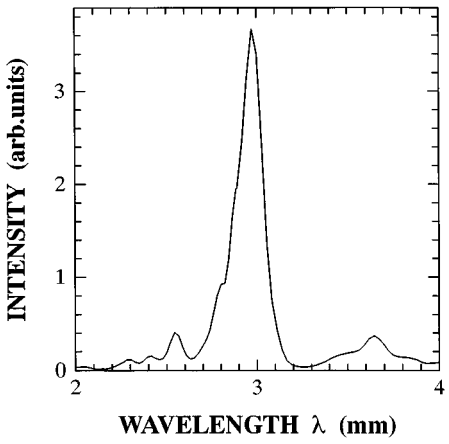

FIG. 7. Spectrum of the coherent SPR at $\lambda = 3.0$ mm. The SPR was emitted from the 40-MeV beam of RRIKU with the grating $G6$ in Table I. The peak width (FWHM) was 0.17 mm.

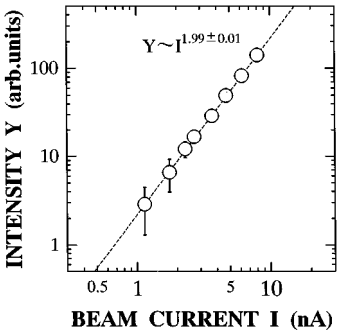

FIG. 8. Dependence of the coherent SPR intensity on the beam current. Electrons were accelerated to 150 MeV by the S-band linac of LNSTU. The straight line is obtained by the least squares method.

B. Coherence effect due to bunched electrons

1. Dependence of intensity on beam current

The dependence of the intensity of SPR on the beam current was measured with the grating $G3$ at $\lambda = 1.3$ mm, using the 150-MeV beam at LNSTU. The beam current was varied by controlling the width of a slit located in a transport system of the beam. The position of the slit was far upstream from the measuring system shown in Fig. 2. The result is shown by open circles in Fig. 8, where the dashed line was fitted by the least squares method. The gradient of the line is 2.0, and the SPR intensity is proportional to the square of the beam current. This confirms that we have observed coherent SPR.

2. Factor of enhancement of intensity and degree of polarization

The intensity of SPR observed with the grating $G2$ from the 150-MeV beam was 0.11 nW at $\lambda = 1.3$ mm and 0.53 nW at $\lambda = 1.6$ mm on a beam current of 10 nA.

To evaluate the bunch form factor $f_L(\lambda)$, or the factor of the enhancement due to the coherence effect $N_e f(\lambda)$ in Eq. (45), we first solved Eqs. (20) and (21) as functions of the emission angles θ and ϕ, and then calculated the intensity of ordinary SPR of Eq. (33) by integrating the solution over the acceptance angle of 50×88 mrad^2.

Figures 9 and 10 show examples of the solutions $|E'_{-1}|^2$ and $|H'_{-1}|^2$ at around $\lambda = 1.3$ mm as functions of the emission angles θ and ϕ. In Fig. 9, the solid curve shows the solution as a function of the angle θ at the azimuth angle of $\phi = 0$. It is shown for the range of the acceptance angle of $\theta \pm 1.43°$ around $\theta = 38.43°$ ($\lambda = 1.3$ mm). In Fig. 10 the open and closed circles show the E- and H-polarized solutions, respectively, as a function of the angle ϕ at the direction of $\theta = 38.43°$. In this figure only the positive part in ϕ is plotted, because the solution is symmetric with respect to $\phi = 0$. In the experiment, the acceptance angle of ϕ was ± 44 mrad. From Fig. 10 we can see that the E- and H-polarized solutions increase rapidly about two orders of magnitude when the angle $|\phi|$ changes within the acceptance angle.

The calculated intensity of incoherent SPR was 1.2×10^{-18} W and 1.4×10^{-18} W at wavelengths of 1.3 and 1.6 mm, respectively. Compared with the calculation, the experimental intensities are enhanced by a factor of 9.2×10^7 at

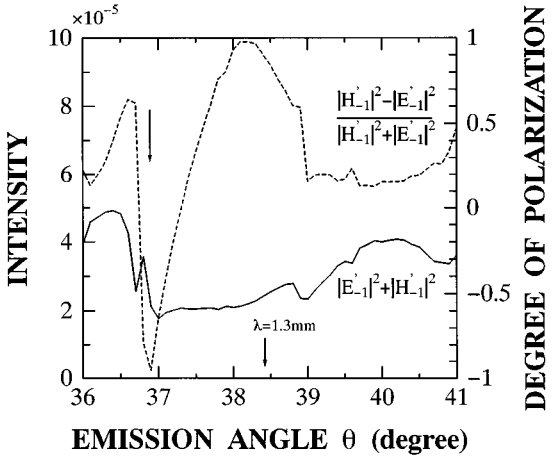

FIG. 9. The solutions $|E'_{-1}|^2$ and $|H'_{-1}|^2$ of Eqs. (20) and (21) as a function of the emission angle θ. The solid curve is $|E'_{-1}|^2+|H'_{-1}|^2$ at $\phi=0$ and the dashed curve shows the degree of polarization, $(|H'_{-1}|^2-|E'_{-1}|^2)/(|H'_{-1}|^2+|E'_{-1}|^2)$.

$\lambda=1.3$ mm and by 3.8×10^8 at $\lambda=1.6$ mm. We consider that these values of the enhancement, $N_e f(\lambda)$ in Eq. (45), are roughly in agreement with the number of electrons in a bunch, $N_e=1.8\times10^8$, taking into account the following uncertainties in the evaluation: the calculated quantities of $|E'_{-1}|^2$ and $|H'_{-1}|^2$ in Eq. (33) were found to be complicated functions of many factors not only of energy but also of $\theta,\phi,\lambda/g,w/g,d/g$, and a small change of these parameters within the experimental conditions occasionally results in a drastic change of the intensity. The acceptance angle of the measuring system was evaluated from the geometry of the system, and has uncertainty due to diffraction, misalignment, and so on. Moreover, the measuring system was calibrated by a point source of blackbody radiation, though SPR has a line source, which may cause an error in addition to the estimated experimental uncertainty of the factor 1.5 in the calibration.

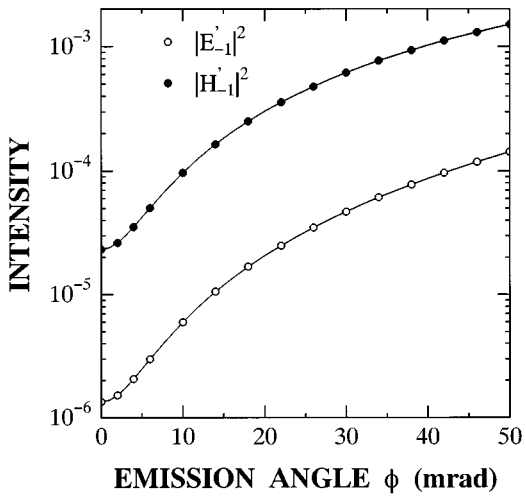

FIG. 10. The solutions $|E'_{-1}|^2$ and $|H'_{-1}|^2$ of Eqs. (20) and (21) as a function of the azimuth angle ϕ at $\theta=38.43°$ ($\lambda=1.3$ mm). The solutions of $|E'_{-1}|^2$ and $|H'_{-1}|^2$ are shown by open and closed circles, respectively.

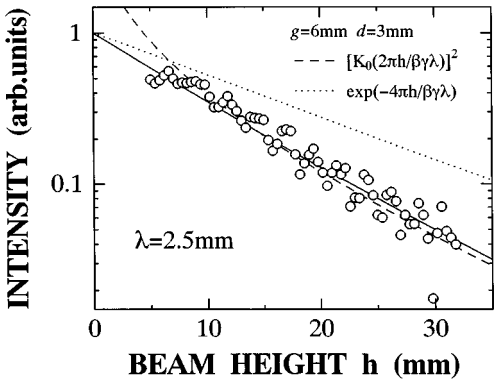

FIG. 11. Dependence of intensity on the beam height at $\lambda=2.5$ mm from the 40-MeV beam of RRIKU. The solid, dashed, and dotted curves are, respectively, the calculated intensity by Eqs. (48) and (49), the theoretical value of the modified Bessel function of $K_0(\xi)^2$ and that of the exponential function of Eq. (2) in the text.

The enhancement of the intensity implies that the bunch form factor derived from the experiment was nearly unity in the millimeter-wave region; $f(\lambda)=f_L(\lambda)f_T(\lambda)\sim1$. This is in agreement with the expected coherence effect for the beam of LNSTU.

SPR was linearly polarized in the plane defined by the grating normal and the trajectory of the beam. The degree of polarization defined by $(I_H-I_V)/(I_H+I_V)$, where I_H and I_V stand for the H- and V-polarized components, respectively, was observed to be 0.6 at the wavelength of 1.3 mm, or at $\theta=38.43°$ with the grating $G2$.

The theoretical degree of polarization is mainly determined by the solutions $|E'_{-1}|^2$ and $|H'_{-1}|^2$ and the theoretical polarization of the solution calculated at $\phi=0$ is shown by the dashed curve in Fig. 9 as a function of the angle θ. At the angle θ of 36.87° $\gamma_n^2(n=-5)$ changes its sign and SPR of the fifth order emerges. The theoretical polarization degree shows rapid variation around θ of 36.87°, caused from redistribution of energy among different orders of SPR. The degree of polarization at $\lambda=1.3$ mm was calculated from Eq. (33) to be 0.50 by integrating each component over the acceptance angle. The value was smaller than the experimental one. We consider, however, that the theoretical value is not in conflict with the experiment, taking into account the rapid variation of the theoretical degree of polarization over the acceptance angle of the optical system.

C. Relativistic effects

1. Dependence of intensity on beam height

Using the 40-MeV beam of RRIKU, we measured the intensity of SPR as a function of the beam height h by moving the grating $G3$ away from the beam trajectory. The results measured at the wavelengths of 2.5 mm are shown by open circles in Fig. 11. The intensity is plotted on a logarithmic scale.

We also measured the dependence using the 150-MeV beam of LNSTU. The Lorentz factor γ of the 150-MeV electron is 293 and it is about four times larger than that of the 40-MeV electron ($\gamma=78$). Figure 12 shows the results obtained at the wavelengths of 1.0 and 2.4 mm, using the grat-

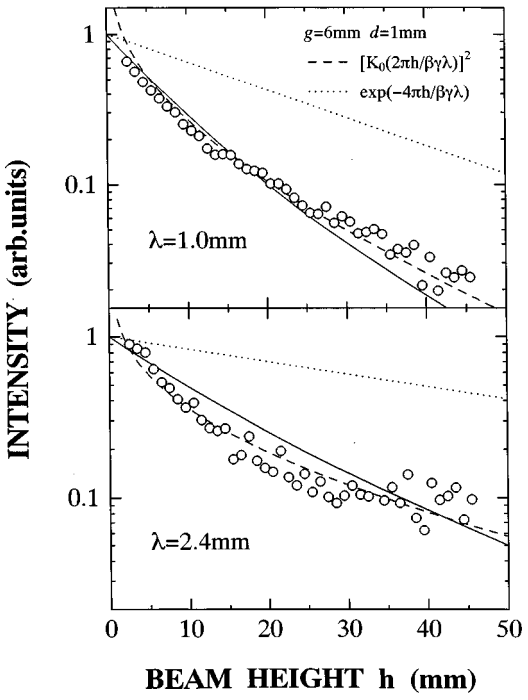

FIG. 12. Dependence of the intensity of coherent SPR on the beam height observed at $\lambda = 1.0$ and 2.4 mm. The energy of the electron was 150 MeV. The solid, dashed, and dotted curves are, respectively, the calculated intensity by Eqs. (48) and (49), the theoretical value of the modified Bessel function of $K_0(\xi)^2$, and that of the exponential function of Eq. (2) in the text.

ing $G2$. The observed intensities are shown by open circles.

In Figs. 11 and 12, the exponential dependence of the intensity on the beam height as in Eq. (2), which was predicted by di Francia [11], is shown by the dotted straight lines. Both figures show that the observed intensities decrease more rapidly than Eq. (2) as the beam height increases. Figure 12 implies that the gradient of the observed intensity approaches that of Eq. (2), only when the beam height increases further.

2. Discussion of the dependence

We discuss the observed dependence considering the acceptance angle of the radiation. The dependence of the electric field of SPR on the beam height h is determined by Eqs. (22) and (23) and is expressed, using Eq. (43), as

$$E_{\omega y}(h) \sim \int_0^{\phi_{\max}} \frac{t}{\sqrt{1+t^2}} \exp(-\xi\sqrt{1+t^2})\, d\phi, \qquad (48)$$

$$H_{\omega y}(h) \sim \int_0^{\phi_{\max}} \exp(-\xi\sqrt{1+t^2})\, d\phi, \qquad (49)$$

where $\xi = 2\pi h/(\beta\gamma\lambda)$, and $t = \beta\gamma \sin\theta \sin\phi$. Equations (48) and (49) should be integrated over the acceptance angle of the measuring system.

We examine the theoretical dependence on the experimental condition that SPR is observed in the plane including the grating normal and the beam trajectory and $\phi \ll 1$. In the case when the energy of the electron is low, i.e., $t \ll 1$, the fields are well approximated by $E_{\omega y}(h) \sim t \exp(-\xi)$ and $H_{\omega y}(h) \sim \exp(-\xi)$. Hence the dependence of the SPR intensity on the beam height is given by Eq. (2). In the case of high energy, on the other hand, t becomes larger than unity even when the emission angle ϕ is small.

We have integrated Eqs. (48) and (49) numerically over the acceptance angle of the measuring system. The energy of SPR, which is normalized to unity at $h = 0$, is proportional to the square of the field, $E_{\omega y}^2 + H_{\omega y}^2$. The results are shown by solid curves in Fig. 11 for the 40-MeV electron at $\lambda = 2.5$ mm, and in Fig. 12 for the 150-MeV beam at $\lambda = 1.0$ and 2.4 mm. The solid curve agrees well with the experimental results. In other words, the results of the observations with the finite acceptance angle are in good agreement with the three-dimensional theory. The intensity-beam height relation is also obtained from integration of Eq. (33): the result is almost the same as the solid curves in Figs. 11 and 12, but shows a little deviation to the upward direction from the solid curves in the range $h > 30$ mm in Fig. 12.

In Figs. 11 and 12, the function $\{K_0(\xi)\}^2$ is also shown by the dashed curves and the radiation intensity is well approximated by $\{K_0(\xi)\}^2$ in a range $h > 1.5\lambda$. This approximation is explained from the expansion of the following series, since the azimuth angle was much smaller than unity, $\phi \ll 1$, in the experiment,

$$\int_0^{\phi_{\max}} \exp(-\xi\sqrt{1+t^2})\, d\phi \sim \int_0^{t_{\max}} \exp[-\xi(1+\tfrac{1}{2}t^2 - \tfrac{1}{8}t^4 + \cdots)]\, dt, \qquad (50)$$

$$K_0(\xi) = \int_0^{\infty} \exp[-\xi \cosh(t)]\, dt \sim \int_0^{\infty} \exp[-\xi(1+\tfrac{1}{2}t^2 + \tfrac{1}{24}t^4 + \cdots)]\, dt. \qquad (51)$$

The comparison of Eqs. (50) and (51) shows that, when the beam height is in such a range that the term $\exp(-\xi t^4)$ and higher ones have minor contributions but the term $\exp(-\xi t^2)$ still has a significant contribution in the integration, the radiation field is approximated by $K_0(\xi)$ and consequently the intensity by $\{K_0(\xi)\}^2$.

When the beam height h increases and the argument of $K_0(\xi)$ becomes large, the modified Bessel function is approximated by an exponential function: $K_0(\xi) \sim \exp(-\xi)$. Therefore for the beam height higher than a certain value, it is difficult to distinguish the relation of $\{K_0(\xi)\}^2$ from that of Eq. (2).

3. Dependence of intensity on azimuth angle

Using the 40-MeV beam, we observed variation of the intensity of SPR by changing the azimuth angle ϕ. Figure 13 shows the results measured with the grating $G3$ at $\lambda = 1.4$ and 1.6 mm: the solid, dashed, and dotted curves show the total intensity and V-polarized and H-polarized components, respectively. The distributions of the intensity were nearly symmetric with respect to the direction of the grating normal, i.e., $\phi = 0$. SPR was emitted in a narrow region including the x-z plane.

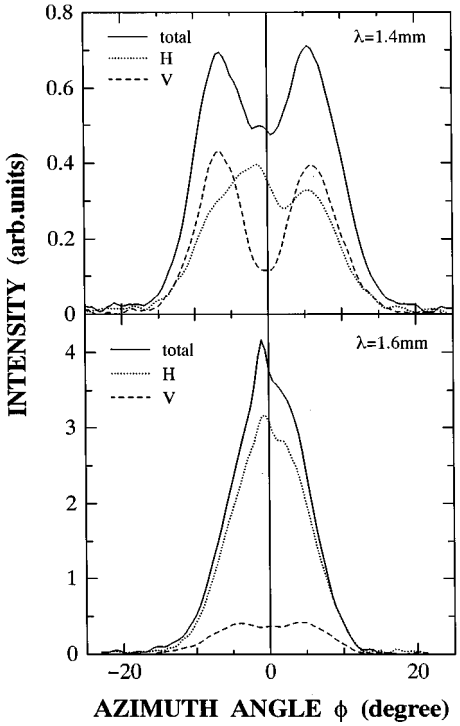

FIG. 13. Dependence of the SPR intensity on the azimuth angle ϕ at $\lambda = 1.4$ and 1.6 mm observed by the 40-MeV beam of RRIKU. The solid, dotted, and dashed curves show the total intensity and the H-polarized and V-polarized components, respectively.

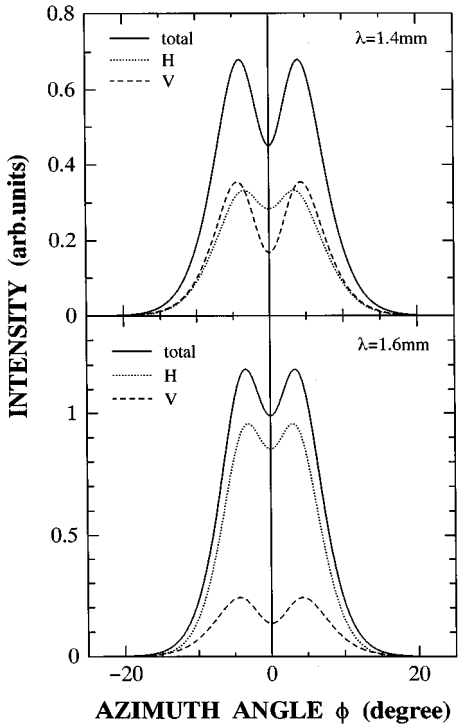

FIG. 14. Theoretical dependence of the SPR intensity from the beam of 40 MeV on the azimuth angle ϕ at $\lambda = 1.4$ and 1.6 mm. The solid, dotted, and dashed curves show the total intensity and the H-polarized and V-polarized components, respectively.

The distribution of V polarization at $\lambda = 1.4$ mm had two peaks, and the angle between the peaks was 12.5°. That of the H polarization also had two peaks but the angle between the two peaks was less than that of the V polarization. On the other hand, at $\lambda = 1.6$ mm the distribution of the V-polarized component had two peaks but the intensity was weak in comparison with that of the H-polarized component. The distribution of the H-polarized component shows no clearly resolved peaks.

We have calculated the theoretical distribution of SPR, taking into account the acceptance angle of the optical system. The results are shown in Fig. 14, where the solid, dashed, and dotted curves show the total intensity, the V-polarized component and the H-polarized component, respectively. All distributions have two peaks, and the calculated intensities decrease rapidly as the azimuth angle $|\phi|$ increases.

The theoretical distribution agrees qualitatively with the experiment. At a wavelength of $\lambda = 1.4$ mm the peak intensity of the H-polarized component is roughly equal to that of the V-polarized one, and the angle between the peak of the H-polarized component is less than that of the V polarization. The central dip of the V-polarized component around at $\phi = 0$ is deeper than that of the H-polarized one. The intensity of the V-polarized component at $\lambda = 1.6$ mm is weaker than that of the H polarization. The width (FWHM) of the theoretical distribution of SPR intensity at $\lambda = 1.4$ mm is 16.2° and wider than that of 14.6° at $\lambda = 1.6$ mm.

There remains, however, small discrepancies between the theory and the experiment: the theoretical distribution of the H-polarized component at $\lambda = 1.6$ mm has two peaks. On the other hand, the experimental one in Fig. 13 has only a central peak with a shoulder. The width (FWHM) of the theoretical concentration of SPR into the x-z plane at $\lambda = 1.4$ mm is narrower than the measured one. On the other hand, the theoretical width at $\lambda = 1.6$ mm is wider than the measured width. The reasons for these discrepancies are not clear at present.

The distributions of the H-polarized component measured at $\lambda = 1.4$ and 1.6 mm have asymmetric structure around at $|\phi| = 0$, while the V-polarized ones are nearly symmetric. The asymmetry is possibly caused by the asymmetric distribution of electrons in the transverse cross section. The asymmetric distribution of electrons, however, hardly disturbs the intensity distribution of the V component, because the V component of SPR is theoretically not emitted into the x-z plane, and the intensity observed within the acceptance angle is weak around $|\phi| \sim 0$.

The sharp decrease of the intensity with the angle $|\phi|$ is expressed by the exponential factor in Eq. (31). In the case of a high energy beam as in the present experiment, i.e., $(\gamma \sin \phi)^2 \gg 1$, the factor reduces to $\exp(-4\pi h|\sin\theta \sin \phi|/\lambda)$ and decreases rapidly with $|\phi|$. The factors $|E'_{-1}|^2$ and $|H'_{-1}|^2$ also depend on the azimuth angle (for example, see Fig. 10). In the case of the high energy beam, the influence of the exponential factor is dominant for the dependence of SPR on the azimuth angle ϕ. The calculation showed, for example, that the factors $|E'_{-1}|^2$ and $|H'_{-1}|^2$ increase four orders of magnitude or more as the angle $|\phi|$ increases from 0 to 90 degrees, while the exponential factor decreases more rapidly with $|\phi|$. Thus the emission of SPR into a narrow direction including the x-z plane is one

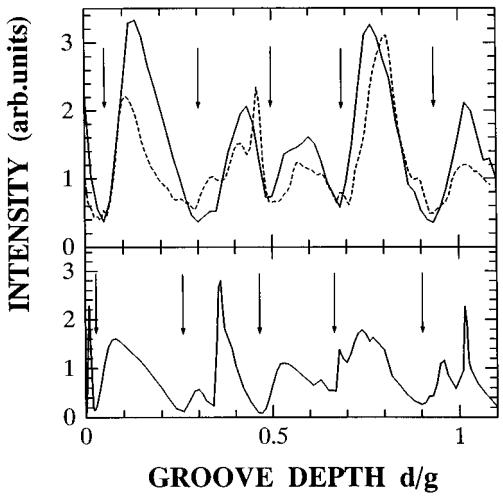

FIG. 15. Dependence of the SPR intensity on the groove depth observed by the 40-MeV beam of RRIKU. The solid curve shows SPR with the 6-mm-period grating at $\lambda = 2.4$ mm and the dashed curve from 12-mm-period grating at $\lambda = 4.8$ mm. The lower part shows the theoretical dependence of the SPR intensity $|E'_{-1}|^2 + |H'_{-1}|^2$ on the groove depth at $\phi = 20$ mrad.

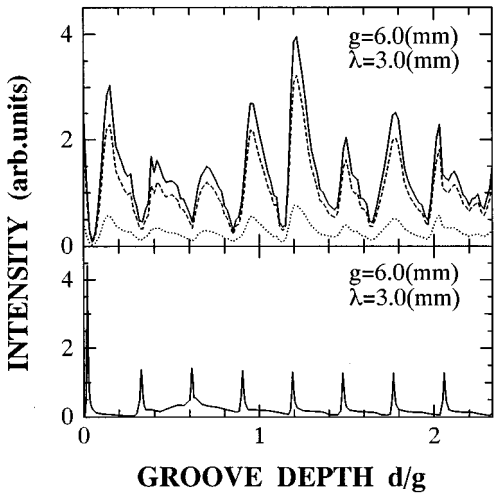

FIG. 16. Dependence of SPR intensity on the groove depth observed at $\lambda = 3$ mm with the lamellar grating $G6$ in Table I. The beam energy is 40 MeV. The lower part shows theoretical dependence of SPR $|E'_{-1}|^2 + |H'_{-1}|^2$ on the groove depth at $\phi = 20$ mrad.

of the properties of the radiation from the relativistic electron. Using the low-energy beam of 100 keV, Gover *et al.* observed that SPR was distributed over a wide range of the azimuth angle from 0 to 70 degrees or more [9].

D. Properties of SPR in relation to grating shape

1. Similarity relation

As pointed out in Section II A, the dependence of SPR intensity at λ on the grating depth will show a similarity to the dependence of SPR at 2λ on the grating depth if all dimensions of the grating are doubled. To confirm such a similarity relation we measured the dependence of the SPR intensity on the groove depth at a wavelength of 2.4 mm with the grating $G6$ and the dependence at $\lambda = 4.8$ mm with $G7$. The period and width of the grating $G7$ are two times larger than those of the grating $G6$.

The results obtained with the 40-MeV beam are shown by the solid curve for $\lambda = 2.4$ mm ($G6$) and by the dashed curve for $\lambda = 4.8$ mm ($G7$) in Fig. 15, where the abscissa is relative depth normalized by the grating period. The ratios $\lambda : g : w : d$ are the same in the two observations.

The solid and dashed curves are similar to each other. Both curves show a structure having five minima indicated by arrows in Fig. 15 with an averaged period of 0.22 in a range from 0.04 to 0.92 in the unit of d/g.

We have simulated the relative variation of the SPR intensity $|E'_{-1}|^2 + |H'_{-1}|^2$ as a function of the groove depth. The result is shown in the lower part of Fig. 15, and has structure similar to the experimental ones. The five minima of the structure were shown by arrows in the range from 0.02 to 0.9 in d/g. The period has been calculated as $0.218 d/g$ by Eq. (52), which is derived in the next section, and is in agreement with the experiment. These results confirm the similarity relation between the wavelength and the grating shape.

Though the calculation reproduced the experimental results qualitatively, there remain small discrepancies. The theoretical depth of grooves, for example, at the minima of SPR intensity indicated by the arrows in Fig. 15 shifted toward the left by about 0.02 in d/g, in comparison with the experiment. The simulation showed two peaks at around $d/g = 1$, but the experiment shows one peak with broad width. The reasons for these discrepancies are not clear at present.

2. Dependence of intensity on groove depth

The dependence of SPR intensity on the depth of the groove was observed, using the 40-MeV beam. Figures 16 and 17 show examples of the observations at the wavelengths λ of 3 and 4.8 mm with the grating $G6$; the solid, dashed, and dotted curves show the total intensity and the H- and V-polarized components, respectively.

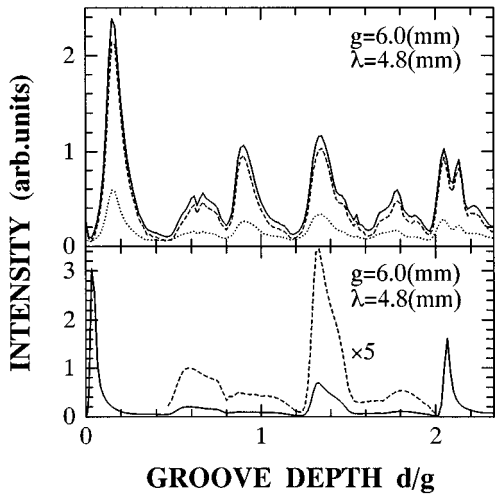

FIG. 17. Dependence of SPR intensity on the groove depth observed at $\lambda = 4.8$ mm with the lamellar grating $G6$ in Table I. The beam energy is 40 MeV. The lower part shows theoretical dependence of SPR, $|E'_{-1}|^2 + |H'_{-1}|^2$, on the groove depth at $\phi = 20$ mrad.

In Figs. 16 and 17, the solid curves of the total intensity change nearly periodically with the groove depth. Periods of the depth are 1.63 mm on average at $\lambda = 3$ mm and 2.34 mm at $\lambda = 4.8$ mm. The degree of polarization was almost independent of the groove depth.

For comparison the SPR intensity $|E'_{-1}|^2 + |H'_{-1}|^2$ has been calculated at $\phi = 20$ mrad as a function of the groove depth, and the results are shown in the lower part of Figs. 16 and 17. To make the distribution clear in Fig. 17, the dashed curve shows five times the intensity in a range from 0.45 to 2 in d/g. The calculation reproduced the periodic change of the observation. The theoretical period is 1.73 mm and 2.45 mm at $\lambda = 3.0$ mm and 4.8 mm, respectively, which are nearly in agreement with the experimental ones, but a little longer.

In Eqs. (20) and (21), the intensity depends on the groove depth d through the factor $\Gamma_m = \exp(i2\kappa_m d)$. Therefore, the dependence shows different behavior according to the value of κ_m. When κ_m is real, the equation of the order m has the same coefficients for different groove depths, $d1$ and $d2$, where $\kappa_m d2 = \kappa_m d1 + K\pi$ is satisfied with an integer K; the solution has periodic structure and the period; i.e., the length of the cycle, Δd, is determined by the relation $\Delta d = \pi/\kappa_m$. This condition is written in the following form in the case where $\phi \ll 1$, which is satisfied in the present experiment:

$$\frac{g}{\Delta d} = 2\left[\left(\frac{g}{\lambda}\right)^2 - \left(\frac{mg}{2w}\right)^2\right]^{1/2}. \tag{52}$$

In our experiment, $g = 2w$ and $m = -1$, and we hence get the period of 1.73 mm from Eq. (52) at $\lambda = 3$ mm. The period corresponds to the periodic structure in Fig. 16.

When κ_m is imaginary, the solution has no periodic structure. Moreover, if $|\kappa_m| d$ is large, Γ_m approaches zero and the solution tends to be independent of the groove depth.

The dependence of SPR on the groove depth becomes complicated when κ_m changes from real to imaginary with an increase in the number $|m|$. Roughly speaking, when the ratio g/λ is large, i.e., the wavelength is short compared with the grating period, SPR of the first order show periodic structure as shown in Fig. 16. On the other hand, if the ratio g/λ is not so large as in the case of $g = 6$ mm and $\lambda = 4.8$ mm, for example, κ_m becomes imaginary for $m = 2$ and the solution of the first order of Eq. (52) does not explain the period of the structure in Fig. 17.

The periodic structure in Fig. 17 is determined by another condition. In Eqs. (20) and (21), the SPR of the order n vanishes at the groove depth where the denominator of the coefficients of E'_n or H'_n becomes zero. This condition is reduced to the following one in the case where $\phi \ll 1$ and for the order $|n| = 1$:

$$\frac{d}{g} = \frac{K}{2[L^2 - (L-1)^2]^{1/2}}, \tag{53}$$

where K is an integer and $L = g/\lambda$. The calculated values of Eq. (53) with $K = 1,2,3, \ldots$ are 0.41, 0.82, 1.22, . . . in d/g, which correspond to the dip of the experiment in Fig. 17.

We consider that the theory has qualitatively reproduced the experimental results, even though there are slight deviations: the theoretical period at $\lambda = 3$ mm, for example, is a little longer than the experimental one. The calculation for the wavelength of 3 mm in the lower part of Fig. 16 shows narrower structure of the peak than the experiment in the upper part. In Fig. 17, the theoretical intensity varies more steeply than the experiment.

When the groove depth is shallow, as clearly shown in Figs. 15–17 the calculation shows that the SPR intensity varies drastically as a function of groove depth. The theoretical distribution of intensity for such a shallow groove depth shows deviation from the experiment. These small but clear discrepancies are to be studied further.

ACKNOWLEDGMENTS

We thank Mr. T. Tsutaya of RISM, Tohoku University, the machine group of TULNS and the staff of KURRI for their technical support and assistance. This work was partially supported by a Grant-in-Aid for Scientific Research from the ministry of Education, Science, and Culture of Japan.

[1] S. J. Smith and E. M. Purcell, Phys. Rev. **92**, 1069 (1953).
[2] K. Ishiguro and T. Tako, Opt. Acta **8**, 25 (1961).
[3] F. S. Rusin and G. D. Bogomolov, Pis'ma Zh. Eksp. Teor. Fiz. **4**, 236 (1966) [JETP Lett. **4**, 160 (1966)].
[4] W. W. Salisbury, J. Opt. Soc. Am. **60**, 1279 (1970).
[5] K. Mizuno, S. Ono, and Y. Shibata, in *Proceedings of the Symposium on Submillimeter Waves* (Polytechnic, New York, 1971), p. 115.
[6] J. P. Bachheimer, Phys. Rev. B **6**, 2985 (1972).
[7] E. L. Burdette and G. Hughes, Phys. Rev. A **14**, 1766 (1976).
[8] S. Suto and M. Ikezawa, Jpn. J. Appl. Phys., Part 1 **22**, 640 (1983).
[9] A. Gover, P. Dvorkis, and U. Elisha, J. Opt. Soc. Am. B **1**, 723 (1984).
[10] I. Shih, W. W. Salisbury, D. L. Masters, and D. B. Chang, J. Opt. Soc. Am. B **7**, 345 (1990).
[11] G. Toraldo di Francia, Nuovo Cimento **16**, 61 (1960).
[12] J. D. Jackson, *Classical Electrodynamics* (Wiley, New York, 1975), Chap. 13.
[13] G. Doucas, J. H. Mulvey, M. Omori, J. Walsh, and M. F. Kimmitt, Phys. Rev. Lett. **69**, 1761 (1992).
[14] K. J. Woods, J. E. Walsh, R. E. Stoner, H. G. Kirk, and R. C. Fernow, Phys. Rev. Lett. **74**, 3803 (1995).
[15] O. Haeberle, P. Rullhusen, J.-M. Salome, and N. Maene, Phys. Rev. E **49**, 3340 (1994).
[16] K. Ishi, Y. Shibata, T. Takahashi, S. Hasebe, M. Ikezawa, K. Takami, T. Matsuyama, K. Kobayashi, and Y. Fujita, Phys. Rev. E **51**, R5212 (1995).
[17] T. Nakazato, M. Oyamada, N. Niimura, S. Urasawa, O. Konno, A. Kagaya, R. Kato, T. Kamiyama, Y. Torizuka, T. Nanba, Y. Kondo, Y. Shibata, K. Ishi, T. Ohsaka, and M. Ikezawa, Phys. Rev. Lett. **63**, 1245 (1989).

[18] Y. Shibata, K. Ishi, T. Ohsaka, H. Mishiro, T. Takahashi, M. Ikezawa, Y. Kondo, T. Nakazato, M. Oyamada, N. Niimura, S. Urasawa, R. Kato, and Y. Torizuka, Nucl. Instrum. Methods Phys. Res. A **301**, 161 (1991).

[19] K. Ishi, Y. Shibata, T. Takahashi, H. Mishiro, T. Ohsaka, M. Ikezawa, Y. Kondo, T. Nakazato, S. Urasawa, N. Niimura, R. Kato, Y. Shibasaki, and M. Oyamada, Phys. Rev. A **43**, 5597 (1991).

[20] U. Happek, A. J. Sievers, and E. B. Blum, Phys. Rev. Lett. **67**, 2962 (1991).

[21] Y. Shibata, K. Ishi, T. Takahashi, T. Kanai, M. Ikezawa, K. Takami, T. Matsuyama, K. Kobayashi, and Y. Fujita, Phys. Rev. A **45**, R8340 (1992).

[22] Y. Shibata, K. Ishi, T. Takahashi, T. Kanai, F. Arai, S. Kimura, T. Ohsaka, M. Ikezawa, Y. Kondo, R. Kato, S. Urasawa, T. Nakazato, S. Niwano, M. Yoshioka, and M. Oyamada, Phys. Rev. E **49**, 785 (1994).

[23] Y. Shibata, S. Hasebe, K. Ishi, T. Takahashi, M. Ikezawa, T. Nakazato, M. Oyamada, S. Urasawa, T. Yamakawa, K. Takami, T. Matsuyama, K. Kobayashi, and Y. Fujita, in *Proceeding of Micro Bunches Workshop*, edited by E. B. Blum, M. Dienes, and J. B. Murphy (AIP Press, New York 1995), p. 473; Y. Shibata, S. Hasebe, K. Ishi, T. Takahashi, M. Ikezawa, T. Nakazato, M. Oyamada, S. Urasawa, and T. Yamakawa, *Proceeding of the Second International Symposium on Radiation of Relativistic Electrons in Periodical Structures*, edited by Yu. L. Pivovarov and A. P. Potylitsin (Cambridge International Science Publishers, Cambridge, 1996), p. 108.

[24] B. M. Bolotovskii and G. V. Voskresenskii, Usp. Fiz. Nauk **94**, 377 (1968) [Sov. Phys. Usp. **11**, 143 (1968)].

[25] P. M. van den Berg, J. Opt. Soc. Am. **63**, 1588 (1973).

[26] P. M. van den Berg and T. H. Tan, J. Opt. Soc. Am. **64**, 325 (1974).

[27] Dr. O. Haeberle derived a similar set of equations in his thesis, Universite Louis Pasteur, 1994 (unpublished). The authors are grateful to Dr. Haebelre for sending his thesis.

[28] N. A. Korkhmazyan, L. A. Gevorgyan, and M. L. Petrosyan, Zh. Tekh. Fiz. **47**, 1583 (1977) [Sov. Phys. Tech. Phys. **22**, 917 (1977)].

[29] Y. Shibata, S. Hasebe, K. Ishi, T. Takahashi, T. Ohsaka, M. Ikezawa, T. Nakazato, M. Oyamada, S. Urasawa, T. Yamakawa, and Y. Kondo, Phys. Rev. E **52**, 6787 (1995).